Structural and Functional Consequences of Binding Site Mutations in Transferrin: Crystal Structures of the Asp63Glu and Arg124Ala Mutants of the N-Lobe of Human Transferrin[†,‡]

Heather M. Baker,[§] Qing-Yu He,[||] Sara K. Briggs,[||] Anne B. Mason,[||] and Edward N. Baker*[,§]

School of Biological Sciences, University of Auckland, Private Bag 92019, Auckland, New Zealand, and Department of Biochemistry, University of Vermont, Burlington, Vermont 05405

Received December 6, 2002; Revised Manuscript Received April 1, 2003

ABSTRACT: Human transferrin is a serum protein whose function is to bind Fe^{3+} with very high affinity and transport it to cells, for delivery by receptor-mediated endocytosis. Structurally, the transferrin molecule is folded into two globular lobes, representing its N-terminal and C-terminal halves, with each lobe possessing a high-affinity iron binding site, in a cleft between two domains. Central to function is a highly conserved set of iron ligands, including an aspartate residue (Asp63 in the N-lobe) that also hydrogen bonds between the two domains and an arginine residue (Arg124 in the N-lobe) that binds an iron-bound carbonate ion. To further probe the roles of these residues, we have determined the crystal structures of the D63E and R124A mutants of the N-terminal half-molecule of human transferrin. The structure of the D63E mutant, determined at 1.9 Å resolution ($R = 0.245$, $R_{free} = 0.261$), showed that the carboxyl group still binds to iron despite the larger size of the Glu side chain, with some slight rearrangement of the first turn of α-helix residues 63−72, to which it is attached. The structure of the R124A mutant, determined at 2.4 Å resolution ($R = 0.219$, $R_{free} = 0.288$), shows that the loss of the arginine side chain results in a 0.3 Å displacement of the carbonate ion, and an accompanying movement of the iron atom. In both mutants, the iron coordination is changed slightly, the principal change being in each case a lengthening of the Fe−N(His249) bond. Both mutants also release iron more readily than the wild type, kinetically and in terms of acid lability of iron binding. We attribute this to more facile protonation of the synergistically bound carbonate ion, in the case of R124A, and to strain resulting from the accommodation of the larger Glu side chain, in the case of D63E. In both cases, the weakened Fe−N(His) bond may also contribute, consistent with protonation of the His ligand being an early intermediate step in iron release, following the protonation of the carbonate ion.

Serum transferrin (Tf)[1] plays a central role in human iron metabolism, by transporting iron in the bloodstream from sites of acquisition to specific cellular receptors. The iron is then delivered to cells by a process involving receptor-mediated endocytosis, release of the transferrin-bound iron at the lower intracellular pH, and recycling of the iron-free apotransferrin back into circulation (*1*, *2*). The requirements for this process are subtle and demanding. The iron is bound with very high affinity, as Fe^{3+}, so that it is generally not available for microbial growth and does not precipitate as insoluble ferric hydroxides, yet mechanisms also exist for the release of this tightly bound iron into cells.

Several reviews have focused on the structure and function of serum transferrin, and the other, homologous, members of the transferrin family, lactoferrin (Lf) and ovotransferrin (oTf) (*3*, *4*). Crystal structures show that in each case the single polypeptide chain of 680−690 amino acid residues is folded into two lobes, the N-lobe and C-lobe, representing its N-terminal and C-terminal halves, respectively. Both lobes have the same fold, consistent with a level of shared sequence identity of ∼40%. Each lobe is folded into two domains of ∼160 residues each (N1 and N2 for the N-lobe, C1 and C2 for the C-lobe), with the two domains in each case enclosing a specific binding site for a single Fe^{3+} ion. Iron release has been shown to involve large-scale domain movements (*5*), with one domain rotating by 50−60° relative to the other, about a hinge near the back of the iron site, such that a transition occurs from the closed, iron-bound state to an open, iron-free state (*6*, *7*).

The nature of the iron binding site is highly conserved, between different transferrins and between the two lobes of each transferrin molecule (*3*). In each case, the Fe^{3+} ion is bound to four amino acid side chains, from Asp, His, and

[†] This work was supported by grants from the U.S. Public Health Service (HD20859 to E.N.B. and DK21739 to A.B.M.), the Marsden Fund of New Zealand, the Health Research Council of New Zealand, and the Wellcome Trust (U.K.) through a Major Equipment Grant.

[‡] Atomic coordinates have been deposited with the Protein Data Bank, as entries 1oqg (D63E mutant) and 1oqh (R124A mutant).

* To whom correspondence should be addressed. Phone: (64) (9) 373-7599, ext 84415. Fax: (64) (9) 373-7619. E-mail: ted.baker@auckland.ac.nz.

[§] University of Auckland.

[||] University of Vermont.

[1] Abbreviations: Tf, transferrin; Lf, lactoferrin; oTf, ovotransferrin; Tf_N, recombinant N-terminal half-molecule of human transferrin (residues 1−337); Lf_N, recombinant N-terminal half-molecule of human lactoferrin (residues 1−334); BHK, baby hamster kidney; PEG, polyethylene glycol; rms, root-mean-square. Mutants of Tf_N or Lf_N are designated by the wild-type amino acid residue, the sequence number, and the amino acid to which the residue was mutated, e.g., D63E.

10.1021/bi020689f CCC: $25.00
Published on Web 05/23/2003

two Tyr residues; in the N-lobe of human Tf, these are Asp63, Tyr94, Tyr188, and His249 (*8*). The same ligand combination is found in virtually every functional transferrin iron binding site, with the exception of the insect transferrins in which the His ligand is often substituted with Gln (*9*). The iron coordination is completed by a synergistically bound CO_3^{2-} ion, which binds in bidentate mode. The CO_3^{2-} ion is itself tightly bound to one domain (N2 or C2) of the protein, through highly favorable hydrogen bonding to two positively charged moieties, an arginine side chain (Arg124 in the N-lobe of human Tf), and the N-terminus of an α-helix. Again, the Arg residue is conserved in all functional iron binding sites. This combination of ligands evidently creates a highly favorable binding site for Fe^{3+}, with appropriate size and charge balance; the +3 charge of the metal ion is balanced by the −3 charge of the Asp and Tyr side chains, and the −2 charge of the carbonate by the positive charges of the Arg side chain and the helix N-terminus (*3*). The result is a very high affinity for Fe^{3+}, with a binding constant of $\sim 10^{20}$. The inclusion of the exogenous carbonate ion in the coordination sphere may facilitate iron release, as structural and functional evidence suggests that protonation of the anion and consequent disruption of its binding mode may be the first step in iron release (*8*).

Several naturally occurring transferrin variants show that mutations of residues in the binding site are in these cases associated with an inhibition of iron binding ability; in the C-lobe of human melanotransferrin, both the Asp ligand and the Arg residue are changed to Ser, and the C-lobe is accordingly unable to bind iron (*10*). Similar mutations to the Asp and Arg residues of the insect transferrin from *Manduca sexta* also produce a C-lobe site that does not bind iron (*11*). Mutagenesis, using the recombinant N-lobe half-molecules of both transferrin and lactoferrin (Tf_N and Lf_N, respectively) as tractable and appropriate model systems (*12*, *13*), has further been used to probe the effect of mutations on the individual components of the binding site. Mutation of the His ligand, for example, has been shown to weaken iron binding and facilitate iron release from both Tf (*14*) and Lf (*15*), and crystal structures of the H249Q mutant of Tf_N (*9*) and the H253M mutant of Lf_N (*15*) have correlated these changes with structural alterations to the metal site.

Here we focus on the Asp ligand, Asp63, and the anion-binding Arg residue, Argl24, in the transferrin N-lobe. Mutations of Asp63 to Ser, Asn, Glu, and Ala all weaken, but do not abolish, iron binding (*16*), but the interpretations in terms of structural perturbations of the iron binding site are not clear. Small-angle X-ray scattering studies suggested that the D63S mutant of Tf_N was in an open conformation (*17*), and the very facile iron release from D63E, similar to that of D63S, suggested that this mutant, too, might not be fully closed, possibly because of misfitting of the larger Glu side chain. On the other hand, the D60S mutant of Lf_N was found by crystallography to be in the closed state but with a water molecule substituting for the mutated Asp ligand (*18*). At the anion binding site, mutation of Arg124 to Ala, Ser, or Lys also leads to much more facile iron release (*19*, *20*), in this case presumably due to destabilization of anion binding, as has also been found for Lf (*21*). Again, how this destabilization is reflected in the structure of the metal or anion state is not known.

Here we present the crystal structures of the D63E and R124A mutants, and show that in both cases the iron-bound form has the normal closed conformation, with no significant change in domain orientation. Adjustments do occur in the metal binding site, however, resulting in both cases in a slightly lengthened Fe−N(His) bond.

MATERIALS AND METHODS

Protein Production. As described previously (*16*, *20*), the R124A and D63E mutants were prepared by PCR-based mutagenesis of a construct that encoded the N-terminal half-molecule of human transferrin, Tf_N, comprising residues 1−337 of the native protein. In both cases, the nucleotide sequences were determined to confirm that the correct mutation had been incorporated, and that no other mutations had been introduced. The recombinant R124A and D63E proteins were then expressed from baby hamster kidney (BHK) cells, containing the relevant cDNA in the pNUT vector, and were purified from the culture medium as previously described (*16*, *20*, *22*). In this protocol, the proteins are obtained in the predominantly iron-saturated form. To ensure full iron saturation, however, and the incorporation of bicarbonate as the synergistic anion, a slight excess of ferric nitrilotriacetate (FeNTA) was added to a buffer solution at pH 7.4, containing the protein and 0.1 M sodium bicarbonate; after standing overnight at 4 °C, the protein solution was then exchanged into 0.1 M ammonium bicarbonate (pH 7.4) by being passed down a gel filtration column.

pH-Dependent Iron Release. The dependence of iron release on pH was determined as previously described for both transferrin and lactoferrin proteins (*13*, *23*). Samples of the fully iron-saturated R124A and D63E proteins were incubated against a series of buffers, chosen to give appropriate buffering over the pH range from 8.0 to 4.0. The protein concentration was in each case 50 μM, and the buffers that were used were HEPES, MES, and sodium acetate, each at a concentration of 50 mM and adjusted to the desired pH by the addition of 1 M sodium hydroxide or acetic acid. Each protein solution was maintained at 4 °C for 7 days, to reach equilibrium, and the percentage of iron remaining at that pH was determined by comparing the absorbance at the visible absorption maximum for that protein (460 nm for R124A and 450 nm for D63E) with that of the fully iron-loaded protein. The data were plotted with a sigmoidal function and analyzed using Origin.

Protein Crystallization. Immediately before crystallization trials were carried out, the protein was passed down a gel filtration column (Superdex 75 HR 10/30), equilibrated in 0.1 M ammonium bicarbonate (pH 7.4). Fractions were tested for monodispersity by dynamic light scattering (Protein Solutions DynaPro-MS200). The Cp/Rh ratio, where Cp is a measure of the size distribution, or polydispersity, and Rh is the mean hydrodynamic radius, was used as an index, and only those samples with a Cp/Rh ratio of <14 were used. Both mutants were crystallized at 18 °C under the same conditions, using the hanging drop method, in which equal volumes of a protein solution [35 mg/mL protein in 0.1 M ammonium bicarbonate (pH 7.4)] and a reservoir solution were mixed. Crystals were obtained by a microseeding method that had been used successfully for other transferrin mutants (*9*, *24*). In this method, a cat's whisker was touched

Table 1: Data Collection and Processing

	D63E	R124A
space group	$P2_12_12_1$	$P2_12_12_1$
cell dimensions (Å)	$a = 44.3$	$a = 43.9$
	$b = 57.2$	$b = 57.1$
	$c = 135.4$	$c = 135.2$
maximum resolution (Å)	1.9	2.4
mosaicity (deg)	0.6	1.0
R_{merge} (%)[a]	5.0 (13.7)	10.0 (43.0)
no. of unique reflections	26077	12875
mean I/σ[a]	20.1 (10.2)	7.4 (2.2)
multiplicity[a]	3.6 (3.6)	3.3 (2.9)
completeness (%)[a]	92.5 (91.1)	91.5 (91.4)

[a] Figures in parentheses are for the outermost shell of data (1.97−1.90 Å for D63E and 2.51−2.40 Å for R124A).

Table 2: Refinement and Model Details

	D63E	R124A
resolution limits (Å)	30.0−1.9	30.0−2.4
no. of reflections[a]	24554 (1250)	11560 (626)
R (R_{free}) (%)	24.5 (26.1)	21.9 (28.8)
model details		
no. of protein atoms	2549	2541
no. of ions	1 Fe^{3+}, 1 CO_3^{2-}, 1 K^+	1 Fe^{3+}, 1 CO_3^{2-}, 1 K^+
no. of water molecules	205	142
rms deviation from standard geometry		
bond lengths (Å)	0.005	0.007
bond angles (deg)	1.3	1.3
residues in most favored regions of the Ramachandran plot (%)	88.0	84.3

[a] All data used, with no σ cutoff. Data used in the R_{free} calculation given in parentheses.

against a previously grown crystal of wild-type $FeTf_N$ and then streaked through a drop of the mutant protein solution that had been previously mixed with an equal volume of reservoir solution. Using a reservoir comprising 0.2 M potassium acetate (pH 7.4) containing 16−22% PEG 3350, high-quality crystals of both mutants could be grown in a few days. For both mutants, the crystals were essentially isomorphous with the form 1 wild-type $FeTf_N$ crystals, with one molecule in the asymmetric unit and the unit cell dimensions given in Table 1.

Data Collection and Processing. X-ray diffraction data were collected from flash-frozen crystals at 110 K, after the crystals had been transferred to a cryoprotectant comprising 0.2 M potassium acetate (pH 7.4) with 35% PEG 3350. Data were collected with Cu Kα radiation ($\lambda = 1.5418$ Å) from a Rigaku RU-300 rotating anode generator equipped with double-focusing mirrors and a Mar345 imaging plate detector. Both data sets were integrated with DENZO and scaled and merged using programs from the CCP4 suite. Data sets were obtained that were more than 90% complete, to maximum resolutions of 1.9 and 2.4 Å for the D63E and R124A mutants, respectively. Full statistics are given in Table 1.

Structure Determination and Refinement. Since the crystals were isomorphous with form 1 wild-type $FeTf_N$ crystals, the 1.6 Å structure of the latter [PDB entry 1A8E (*8*)] was used to derive an initial model for each mutant. All solvent molecules and the Fe^{3+} and CO_3^{2-} ions were removed, and the mutated residue (Asp63 in D63E and Arg124 in R124A) was in each case truncated to Ala. The same refinement protocol was then followed for each mutant. Rigid body refinement, first as the whole molecule and then as the two domains, was carried out with CNS (*25*) and followed by simulated annealing between 10 000 and 100 K. For all subsequent model building, SIGMAA-weighted $2mF_o - DF_c$ and $mF_o - DF_c$ difference electron density maps were used, and were interpreted using the TURBO FRODO graphics package (*26*) on a Silicon Graphics workstation. The positions of the ferric and carbonate ions, and the conformations of the mutated residues, were clearly apparent, and these groups were added to the model immediately, although they and the other residues of the iron coordination sphere were checked several times in "omit" maps during the subsequent structure refinement, during which CNS was again used. Solvent molecules were added using the automatic solvent addition procedures in CNS, but were visually checked in difference maps, and only those with good spherical density, reasonable *B*-factors, and hydrogen bond partners with appropriate geometry were retained in the model. All were treated as water molecules, except for one potassium ion that had been found in other $FeTf_N$ structures (*24*), and its identity verified from its environment and from refinement. The final values for R and R_{free} were 24.5 and 26.1%, respectively, for D63E and 21.9 and 28.8%, respectively, for R124A, with approximately 5% of reflections, randomly chosen, used in the R_{free} calculation (*27*). Full refinement and model statistics are given in Table 2.

Model Completeness and Quality. The final model consisted of residues 3−331 for both mutants, with no electron density being apparent for the N-terminal residues prior to Asp3 or for the C-terminal residues following Cys331. The protein molecules conform well with standard geometry. Bond lengths and angles are restrained close to the standard values of Engh and Huber (*28*) (Table 2), and the polypeptide chain torsion angles conform with allowed regions of the Ramachandran plot; for D63E, 88.0% of residues are in the most favored regions, as defined by PROCHECK (*29*), and for R124A, the figure is 84.3%.

RESULTS AND DISCUSSION

Overall Molecular Conformation. Neither of the mutations reported here has any effect on the overall folding of the iron-loaded half-molecule, shown in Figure 1, or on the extent of domain closure. In both mutants, as in wild-type $FeTf_N$, the two domains (N1 and N2) are fully closed over the iron atom. Superpositions of each mutant structure onto wild-type Tf_N show that in both cases the root-mean-square (rms) difference in Cα positions is virtually the same for the complete half-molecule as it is for its two constituent domains, implying no significant difference in domain orientations. For D63E, the rms difference is 0.28 Å for the whole N-lobe, compared with values of 0.32 and 0.23 Å for its N1 and N2 domains, respectively, and for R124A, the corresponding figures are 0.36 (whole lobe), 0.38 (N1 domain), and 0.27 Å (N2 domain). Differences in domain rotation, computed by first superimposing one pair of domains and then seeing what rotation was required to bring the other pair of domains into coincidence, are less than 0.4° for both mutants.

The D63E mutation was expected to compromise both domain closure and the strength of interdomain interactions. In wild-type $FeTf_N$, Asp63 plays a critical role by coordinating the iron through one carboxylate oxygen, and through its other carboxylate oxygen forming a short (2.8 Å),

FIGURE 1: Polypeptide folding of the N-lobe half-molecule of human transferrin (Tf_N). The bound iron atom is shown as a red sphere and the carbonate ion in orange, and the side chains of Asp63 and Arg124 are shown in magenta. This figure was drawn with MOLSCRIPT (*33*) and rendered with Raster3D (*34*).

geometrically favorable, hydrogen bond with the main chain nitrogen of Thr125 in the opposing domain (*3*, *8*). These intimate interactions would seem to leave little room for the bulk of an extra methylene group in the side chain. Surprisingly, in the mutant described here, G1u63 makes the same interactions as Asp63 and the domain closure is unchanged; its carboxylate group coordinates the iron through Oϵ1 (2.02 Å) and hydrogen bonds to the NH group of Thr125 (2.9 Å) through Oϵ2. When the wild-type and D63E crystal structures are superimposed the carboxylate oxygen positions for Asp63 and G1u63 differ by less than 0.2 Å (Figure 2A). The ability to tolerate this substitution seems to depend on some plasticity at the N-terminus of the α-helix formed by residues 63−72. Shifts of 0.4−0.8 Å occur in residues 62−65, with a maximum of 0.8 Å for Cα of G1u63, and there are small changes in main chain torsion angles (less than 10°). These distortions result in the loss of two weak hydrogen bonds (the 64O···68N distance increases from 3.4 to 3.9 Å and the 65O···69N distance from 3.4 to 4.0 Å), and the carbonyl oxygen atom of residue 65 is left without a hydrogen bond partner. A distortion of this helix is also seen in lactoferrin in response to the related D60S substitution (*18*).

The lack of any change in domain orientations is less surprising for R124A than for D63E, because the Arg124 side chain in wild-type $FeTf_N$ is not involved in any direct, or even water-mediated, interdomain interactions. On the other hand, because the guanidinium group of Arg124 is a key component of the anion binding site, and thus indirectly of the strong iron-mediated bridge between the domains, the lack of any change in domain closure must reflect the general constancy in the metal binding site (see below).

Other features of the three-dimensional structure of $FeTf_N$ are also preserved in the two mutants. The unusual "dilysine pair" interaction in $FeTf_N$ [a 3.01 Å hydrogen bond between the ϵ-amino groups of Lys206 and Lys296 (*8*)] is present in both D63E and R124A, where the corresponding distances are 2.94 and 3.11 Å, respectively. Cation−π interactions involving a cluster of aromatic groups that surround these two lysines are also conserved. Many of the well-ordered solvent sites also match, including that of the bound potassium ion in the surface of the N2 domain.

Metal and Anion Binding Sites. In the binding sites of both mutants, the iron coordination and anion hydrogen bonding remain very much the same as in wild-type $FeTf_N$. The iron atom in each case remains six-coordinate, with the same set of ligands (two Tyr residues, one His residue, one carboxylate, and a bidentate carbonate ion), and bond distances that are in most cases unchanged (Table 3). The changes that do take place can be traced primarily to small displacements of one or more (but not all) of the ligands, with the iron atoms following. These movements, which presumably originate from the mutations, subtly alter the site and may thus propagate to changes in iron binding behavior.

In the D63E mutant, the principal changes stem from a small shift (0.1−0.2 Å) of the carboxylate oxygens of G1u63, relative to Asp63 in wild-type $FeTf_N$. Although the Fe−O

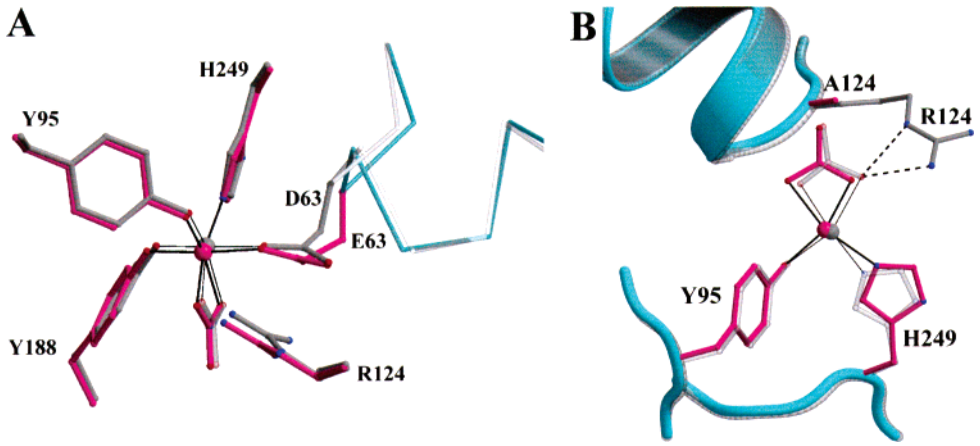

FIGURE 2: Superposition of (A) the D63E structure and (B) the R124A structure on wild-type Tf_N. In each case, the mutant is shown with the polypeptide in blue and the side chains, iron atom, and carbonate ion in magenta, whereas wild-type Tf_N is in gray. In panel A, the iron coordination and the small structural disturbances associated with the Asp63Glu mutation are shown. The larger Glu side chain is accommodated through distortion of the first turn of the α-helix, residues 63−72 (right), and a small displacement of the iron atom. In panel B, the displacement of the carbonate ion in the mutant, following the loss of the guanidinium group of Argl24, is shown, with the consequent shift in the iron atom and lengthening of the Fe−N(His) bond. The iron ligands Asp63 (below the iron) and Tyr188 (above the iron) are omitted for clarity. This figure was drawn with MOLSCRIPT (*33*) and rendered with Raster3D (*34*).

Table 3: Metal−Ligand Bond Lengths and Anion−Protein Hydrogen Bonds (Å)

	$FeTf_N$[a]	D63E	R124A
Fe−Oδ1(Asp63)	2.02	2.02[b]	2.14
Fe−Oη(Tyr95)	1.99	1.88	1.97
Fe−Oη(Tyr188)	1.90	2.00	2.08
Fe−Nϵ2(His249)	2.10	2.22	2.38
Fe−O1(CO_3^{2-})	2.24	2.13	2.01
Fe−O2(CO_3^{2-})	2.06	2.05	2.24
O1−Nη2(Arg124)	2.57	2.73	−
O1−Nϵ(Arg124)	2.81	2.95	−
O2−N(A1a126)	3.02	2.86	2.72
O3−N(Gly127)	2.97	2.89	3.04
O3−Oγ1(Thr120)	2.63	2.64	2.75

[a] Data from the form 1 high-pH structure for wild-type $FeTf_N$. [b] Bond to atom Oϵ1 of Glu63.

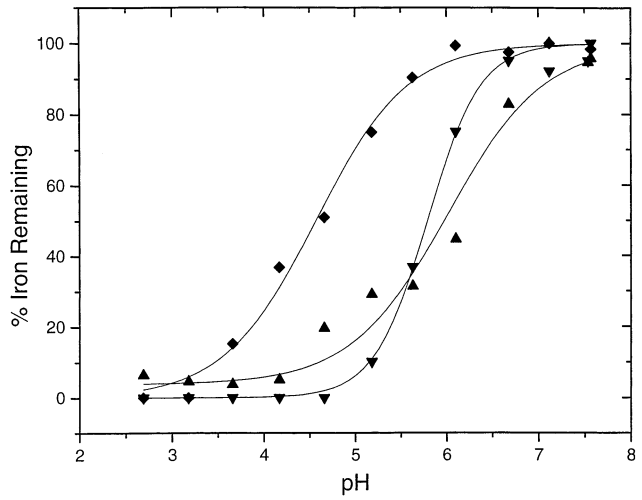

FIGURE 3: pH profiles showing the loss of iron as the pH is lowered from 7.6 to 2.7 [wild-type Tf_N (◆), R124A mutant (▲), and D63E mutant (▼)]. The solid lines in each case show the fit to a sigmoidal function, which is good for wild-type and D63E proteins but not for R124A (see the text).

bond length is unchanged, and the same hydrogen bonds are made by G1u63 and Asp63, the movement displaces the iron atom by ~0.2 Å, in a direction away from the N1 domain, and hence away from His249, lengthening the Fe−N(His249) bond (Figure 2A). The carbonate ion also moves with the iron atom, and there are small changes in the other metal−ligand bond lengths.

In the R124A mutant, the loss of the guanidinium group of Argl24, which in wild-type $FeTf_N$ forms one wall of the anion binding site, causes the carbonate ion to be displaced 0.3 Å from its wild-type position (Figure 2B). The movement is in a direction away from the arginine position, toward residues 124−128 which, as the N-terminal turn of helix 5, form the remainder of the anion binding site. The iron atom moves with the carbonate ion, in a direction away from the two ligands that are contributed by the N1 domain, His249 and Asp63. The major difference is in the Fe−N(His) bond, which is lengthened by ~0.3 Å, to 2.4 Å. Thus, changes in the anion position propagate to this change in the iron−histidine coordination.

Iron Binding and Release. Functional studies of the N-terminal half-molecule of human transferrin have already shown that mutations of both Asp63 and Argl24 weaken iron binding and accelerate iron release (*19*, *20*, *30*, *31*). Although not all of these studies have been carried out under identical conditions of pH, buffer, salt concentration, or added chelator, a consistent pattern nevertheless emerges. In a kinetic analysis of mutations to Asp63, He et al. (*30*) showed that for four Asp63 mutants (D63E, D63S, D63N, and D63A) iron release to the chelator EDTA was greatly accelerated compared with that in the wild type, with the relative rates being in the following order: D63E ~ D63S < D63N ~ D63A. At pH 7.4, using the chelator Tiron, these four mutants all released iron more than 1000 times faster than the wild type (*31*). Likewise, two studies of mutations to Arg124 indicate accelerations in iron release of 50−100-fold when this residue is mutated to Ala or Ser (*19*, *20*, *31*).

The ability of the protein to retain iron to low pH is also compromised by mutations of these two residues. As the pH is lowered, both mutants lose iron more than 1 pH unit higher than does wild-type Tf_N, when the iron retention experiment is carried out in parallel for Tf_N, D63E, and R124A, under identical solution conditions of buffer, salt, and protein concentration (Figure 3). A measure of these differences can be taken from the values of pH_{50}, the pH at which 50% of the iron has been released. Here the pH_{50} values are 4.7 for Tf_N, 5.8 for D63E, and 6.1 for R124A, indicating that for both mutants protonation much more readily stimulates iron release. Similar observations have been made for mutants of the N-lobe half-molecule of lactoferrin, where mutations of the equivalent Arg121 to Ser and Glu, and of Asp60 to Ser, destabilized iron binding substantially relative to that of wild-type Lf_N (*18*, *21*). For these mutants, iron release began at a significantly higher pH than it did for wild-type Lf_N, pH ~7.0−7.5 versus pH 5.0−5.5 for wild-type Lf_N. Both wild-type Tf_N and the D63E mutant fit well to a sigmoidal iron release curve. Intriguingly, this is not true of R124A (see Figure 3). The explanation is not clear, but it is possible that this mutant may be present in two distinct species, with separate end points, only one of which is captured in the crystal. Alternative configurations for the CO_3^{2-} ion, as seen for wild-type Tf_N at pH ~6 (*8*), may be one possibility.

These structural results show that there is sufficient plasticity in the iron binding site and its immediate environment to accommodate substitutions without compromising the closed structure of the iron-loaded form of the protein. Thus, the decreased iron binding stability and more facile iron release of the D63E mutant are not the result of a more open cleft caused by the extra bulk of the G1u63 residue at a critical point between the domains. Instead, the closed structure is maintained, at the expense of some distortion in the α-helix (residues 63−72) that carries this residue. A similar result was found for the related D60S mutant of lactoferrin, where distortion of the same helix allowed a water molecule to take the place of the aspartate ligand, and a closed structure to be maintained (*18*). In fact, all the iron-loaded transferrins that have been analyzed crystallographically to date, both mutants and wild type, have been found to adopt a fully domain-closed structure, albeit with small internal adjustments in some individual mutants. Relevant to this is the fact that all the mutants analyzed to date have been crystallized at a pH above that at which iron is lost in solution; here both the D63E and R124A mutants were crystallized at pH 7.4, considerably higher than the pH at which iron is lost.

What then is responsible for the reduced stability of iron binding and faster release seen for the two mutants examined here? In the case of R124A, the loss of the positively charged arginine side chain, which forms one wall of the anion binding site and donates two hydrogen bonds to the carbonate ion, must raise the pK_a of the carbonate ion, making it more readily protonated. This is probably the main reason for the reduced stability of the R124A mutant, consistent with the view that protonation of the carbonate ion is a critical first step toward iron release (*8*). Similar conclusions come from a structure−function analysis of two related lactoferrin mutants, R121S and R121E (*21*). In the R124A mutant described herein, the lengthened bond to the histidine ligand, His249, probably also plays a part. This must reduce the stability of iron binding, a phenomenon that also occurs when histidine is substituted with other amino acids, and it is likely to make the histidine more susceptible to protonation. Kinetic studies have suggested that protonation of the histidine ligand is an intermediate step in the mechanism of iron release from transferrin, following the initial protonation of the carbonate ion (*32*).

In the case of the D63E mutant, the likely reasons for its reduced level of iron binding and more facile release, compared with those of the wild type, must be more subtle. Again, the Fe−N(His) bond is lengthened slightly, and this may weaken binding. However, the distortions in the helix to which residue 63 is attached, and the accompanying loss of intrahelix hydrogen bonding, are the price that is paid for maintenance of iron binding in a domain-closed structure, and these may be the most significant factor. These distortions could be seen as a "thermodynamic tension" in the iron-loaded, domain-closed structure, which would be released when iron is lost.

CONCLUSIONS

The D63E and R124A mutations alter the iron binding site and the anion binding site, respectively, in the N-lobe of human transferrin. Both mutations substantially weaken iron binding, as is evident from the more rapid iron release, and substantially decreased stability to acid of the mutant proteins. In contrast, the D63E and R124A mutant proteins are remarkably similar to the wild-type molecule in three-dimensional structure, with only small perturbations of the binding site apparent. In the case of the R124A substitution, this suggests that destabilization of iron binding results primarily from the increased susceptibility to protonation of the carbonate ion following the loss of the arginine side chain, and possibly also from an accompanying small structural perturbation that weakens the Fe−His bond. Only small local distortions result from the D63E substitution, reflecting the strong preference of transferrin for a single domain-closed structure, and the relative plasticity of protein structures in accommodating single residue changes. We suggest, however, that these same distortions also destabilize iron binding in this mutant, by making it more susceptible to domain opening.

REFERENCES

1. Klausner, R. D., Ashwell, J. V., Van Renswoude, J. B., Harford, J., and Bridges, K. (1983) *Proc. Natl. Acad. Sci. U.S.A. 80*, 2263−2267.
2. Aisen, P. (1998) *Met. Ions Biol. Syst. 35*, 585−631.
3. Baker, E. N. (1994) *Adv. Inorg. Chem. 41*, 389−463.
4. Aisen, R., and Harris, D. C. (1989) in *Iron carriers and iron proteins* (Loehr, T., Ed.) pp 241−351, VCH Publishers, New York.
5. Grossmann, J. G., Neu, M., Pantos, E., Schwab, F. J., Evans, R. W., Towns-Andrews, E., Lindley, P. F., Appel, H., Thies, W.-G., and Hasnain, S. S. (1992) *J. Mol. Biol. 225*, 811−819.
6. Anderson, B. F., Baker, H. M., Norris, G. E., Rumball, S. V., and Baker, E. N. (1990) *Nature 344*, 784−787.
7. Jeffrey, P. D., Bewley, M. C., MacGillivray, R. T. A., Mason, A. B., Woodworth, R. C., and Baker, E. N. (1998) *Biochemistry 37*, 13978−13986.
8. MacGillivray, R. T. A., Moore, S. A., Chen, J., Anderson, B. F., Baker, H., Luo, Y., Bewley, M., Smith, C. A., Murphy, M. E., Wang, Y., Mason, A. B., Woodworth, R. C., Brayer, G., and Baker, E. (1998) *Biochemistry 37*, 7919−7928.
9. Baker, H. M., Mason, A. B., He, Q.-Y., and Baker, E. N. (2001) *Biochemistry 40*, 11670−11675.
10. Baker, E. N., Baker, H. M., Smith, C. A., Stebbins, M. R., Kahn, M., Hellstrom, K. E., and Hellstrom, I. (1992) *FEBS Lett. 298*, 215−218.
11. Bartfeld, N. S., and Law, J. H. (1990) *J. Biol. Chem. 265*, 21684−21691.
12. Funk, W. D., MacGillivray, R. T. A., Mason, A. B., Brown, S. A., and Woodworth, R. C. (1990) *Biochemistry 29*, 1654−1660.
13. Day, C. L., Stowell, K. M., Baker, E. N., and Tweedie, J. W. (1992) *J. Biol. Chem. 267*, 13857−13862.
14. He, Q.-Y., Mason, A. B., Pakdaman, R., Chasteen, N. D., Dixon, B. K., Tam, B. M., Nguyen, V., MacGillivray, R. T. A., and Woodworth, R. C. (2000) *Biochemistry 39*, 1205−1210.
15. Nicholson, H., Anderson, B. F., Bland, T., Shewry, S. C., Tweedie, J. W., and Baker, E. N. (1997) *Biochemistry 36*, 341−346.
16. He, Q.-Y., Mason, A. B., Woodworth, R. C., Tam, B. M., Wadsworth, T., and MacGillivray, R. T. A. (1997) *Biochemistry 36*, 5522−5528.
17. Grossmann, J. G., Mason, A. B., Woodworth, R. C., Neu, M., Lindley, P. F., and Hasnain, S. S. (1993) *J. Mol. Biol. 231*, 554−558.
18. Faber, H. R., Bland, T., Day, C. L., Norris, G. E., Tweedie, J. W., and Baker, E. N. (1996) *J. Mol. Biol. 256*, 352−363.
19. Zak, O., Aisen, P., Crawley, J. B., Joannou, C. L., Patel, K. J., Rafiq, M., and Evans, R. W. (1995) *Biochemistry 34*, 14428−14434.
20. He, Q.-Y., Mason, A. B., Nguyen, V., MacGillivray, R. T. A., and Woodworth, R. C. (2000) *Biochem. J. 350*, 909−915.
21. Faber, H. R., Baker, C. J., Day, C. L., Tweedie, J. W., and Baker, E. N. (1996) *Biochemistry 35*, 14473−14479.
22. Woodworth, R. C., Mason, A. B., Funk, W. D., and MacGillivray, R. T. A. (1991) *Biochemistry 30*, 10824−10829.
23. MacGillivray, R. T. A., Bewley, M. C., Smith, C. A., He, Q.-Y., Mason, A. B., Woodworth, R. C., and Baker, E. N. (2000) *Biochemistry 39*, 1211−1216.
24. Nurizzo, D., Baker, H. M., He, Q.-Y., MacGillivray, R. T. A., Mason, A. B., Woodworth, R. C., and Baker, E. N. (2001) *Biochemistry 40*, 1616−1623.
25. Brunger, A. T., Adams, P. D., Clore, G. M., DeLano, W. L., Gros, P., Grosse-Kunstleve, R. W., Jiang, J. S., Kuszewski, J., Nilges, M., Pannu, N. S., Read, R. J., Rice, L. M., Simonson, T., and Warren, G. L. (1998) *Acta Crystallogr. D54*, 905−921.
26. Cambillau, C., Roussel, A., Inisan, A.-G., and Knoops-Mouthuy, E. (1996) *Bio-Graphics*, AFMB-CNRS, Marseille, France.
27. Brunger, A. T. (1992) *Nature 355*, 472−474.
28. Engh, R. A., and Huber, R. (1991) *Acta Crystallogr. A47*, 392−400.
29. Laskowski, R., MacArthur, M., Moss, D., and Thornton, J. M. (1993) *J. Appl. Crystallogr. 26*, 283−291.
30. He, Q.-Y., Mason, A. B., and Woodworth, R. C. (1997) *Biochem. J. 328*, 439−445.
31. He, Q.-Y., and Mason, A. B. (2002) in *Molecular and Cellular Iron Transport* (Templeton, D. M., Ed.) pp 95−123, Marcel Dekker, New York.
32. el Hage Chahine, J. M., and Pakdaman, R. (1995) *Eur. J. Biochem. 230*, 1102−1110.
33. Kraulis, P. J. (1991) *J. Appl. Crystallogr. 24*, 946−950.
34. Merritt, E. A., and Bacon, D. J. (1997) *Methods Enzymol. 277*, 505−524.

BI020689F